Scaling Behavior of Barkhausen Avalanches along the Hysteresis loop in Nucleation-Mediated Magnetization Reversal Process

M.-Y. Im[1,3], P. Fischer[1], D.-H. Kim[2], and S.-C. Shin[3*]

[1]Center for X-ray Optics, Lawrence Berkeley National Laboratory, Berkeley CA94720, USA

[2]Department of Physics, Chungbuk National University, Cheongju 361-763, South Korea

[3] Department of Physics and Center for Nanospinics of Spintronic Materials, Korea Advanced Institute of Science and Technology, Daejeon 305-701, Korea

Abstract

We report the scaling behavior of Barkhausen avalanches for every small field step along the hysteresis loop in CoCrPt alloy film having perpendicular magnetic anisotropy. Individual Barkhausen avalanche is directly observed utilizing a high-resolution soft X-ray microscopy that provides real space images with a spatial resolution of 15 nm. Barkhausen avalanches are found to exhibit power-law scaling behavior at all field steps along the hysteresis loop, despite their different patterns for each field step. Surprisingly, the scaling exponent of the power-law distribution of Barkhausen avalanches is abruptly altered from 1 ± 0.04 to 1.47 ± 0.03 as the field step is close to the coercive field. The contribution of coupling among adjacent domains to Barkhausen avalanche process affects the sudden change of the scaling behavior observed at the coercivity-field region on the hysteresis loop of CoCrPt alloy film.

Magnetization reversal in a ferromagnetic material under an external magnetic field occurs via a series of discrete and sudden magnetization change, known as the Barkhausen avalanche [1]. Recent studies on Barkhausen avalanches of 2D and 3D ferromagnetic materials reveal non-trivial fluctuation of the power-law scaling behavior [2-9], as observed in a wide variety of physical phenomena including metal-insulator transition [10], earthquakes [5], superconductor vortices [11], and charge density waves [12]. The Barkhausen avalanche is considered as a crucial phenomenon fundamentally related with the hysteresis in magnetization reversal process, which is a century-old scientific question in magnetism and also a key technological issue in achieving reliability of magnetic recording [13-17]. Therefore, to fully understand fundamental phenomena in the hysteresis, a systematic study on the statistical behavior of Barkhausen avalanches at every small field step along the hysteresis loop is necessary. In particular, the study on 2D ferromagnetic films with perpendicular magnetic anisotropy (PMA) is very important, since the magnetization reversal in those systems is accompanied with magnetic domain nucleation, domain growth, domain wall motion, and their interaction on the hysteretic cycle [17-19]. So far, much theoretical studies have devoted to understand a phenomenon of hysteresis based on an examination of Barkhausen avalanches on hysteretic cycle [5,6,13-16,20-22] and a few of them have investigated on Barkhausen avalanches in magnetization reversal by domain nucleation and growth [2,5,16]. However, theoretical model ranging over an extensive reversal process from domain nucleation to domain wall motion is still lacking.

So far, most experimental studies have been carried out on in-plane anisotropic materials revealing domain-wall mediated magnetization reversal process, which provide large Barkhausen jump sizes easily detectable by classical inductive method or magneto-optical Kerr effect technique [3,6,7-9]. Also, the experiments were performed only in the critical field region around the coercive field or to examine ensemble averaged statistical behavior of Barkhausen avalanches on an entire hysteresis loop [7-9,23]. But, almost no experiments have been done on Barkhausen avalanches in nucleation-mediated magnetization reversal process, mainly due to low sensitivity and spatial resolution of the available measurement techniques. Thus, the direct observation of Barkhausen avalanches at every small field step in the hysteretic cycle in nucleation-mediated

magnetization reversal process, together with its statistical analysis, has remained a scientific challenge to date. In this Letter we have investigated the statistical behavior of Barkhausen avalanches for each field step along the hysteresis loop of CoCrPt alloy film having PMA, which is one of the promising candidates as a high-density perpendicular magnetic recording medium [24-26], by means of the magnetic soft X-ray transmission microscopy (MTXM) with a high spatial resolution of 15 nm [27-28].

Direct observation of magnetic domain configuration was carried out using the full-field magnetic transmission soft X-ray microscopy beamline 6.1.2 at the Advanced Light Source in Berkeley CA. Details of this X-ray microscope setup were described elsewhere [29]. A condensor zone plate (CZP) together with a pinhole close to the specimen serves as a linear monochromator due to the wavelength dependence of the focal length of the CZP, which provides the selective X-rays with energy corresponded to Ni L_3 (854 eV), Co L_3 (777 eV), and Fe L_3 (706 eV) absorption edge, etc. After transmitting the circularly polarized X-ray through the sample, the image is projected by the micro zone plate (MZP) objective lens to a 2048 × 2048 pixel backside illuminated CCD. Magnetic contrast is achieved by X-ray magnetic circular dichroism (XMCD). 50-nm thick $(Co_{0.83}Cr_{0.17})_{87}Pt_{13}$ alloy film was prepared on a 40-nm thick Ti buffer layer using dc magnetron cosputtering of CoCr alloy target and Pt target at a base pressure better than 8 × 10^{-7} Torr and at sputtering Ar pressure of 3 mTorr in ambient temperature. The magnetic easy axis of the film determined using a torque magnetometer was confirmed to be normal to the film plane. A 200-nm thick Si_3N_4 membrane substrate was used to allow the high transmission of soft X-ray. Microstructual and macroscopic magnetic properties of the sample were characterized by a transmission electron microscope (TEM) and a vibrating sample magnetometer (VSM), respectively.

Magnetic domain images of CoCrPt alloy film were recorded at the Co L_3 (777 eV) absorption edge with varying the external magnetic field orientating normal to the sample plane. The measurement time during the X-ray experiment took usually ~1 sec to get a single-shot full-field image. The images were normalized by a saturated image taken under sufficient external field to distinguish magnetic contrast from structural one. The sample was initially saturated with a positive maximum field and then a reversing field was applied to trigger magnetic domain nucleation and magnetization reversal. Fig. 1

shows magnetic domain configurations of CoCrPt film taken at external fields of +600, +400, +200, 0 and -200 Oe along the hysteresis loop together with M-H curve measured by VSM, where domain configurations are observed at an exactly identical sample area. The typical nucleation-mediated magnetization reversal process in this system is clearly witnessed in Fig.1. It can be seen that new domains are randomly appeared at many nucleation sites with the variation of an applied field from +600 to +400 Oe, designated as the field step I. It is found that the size of newly nucleated domains is $\lesssim$ 40 nm, following a Gaussian statistical distribution. Considering the fact that the grain size also follows a Gaussian distribution with the average size of ~ 30 nm [30], the nucleation-mediated reversal process in this system is believed to carried out via individual switching of grains segregated by higher Cr composition at grain boundaries. As an applied magnetic field changes from +400 to +200 Oe (the field step II) along the descending branch of the hysteresis loop, the small nucleated domains are grown with irregular shape, while new domains are form at the other nucleation sites. With an applied field approaching 0 from +200 Oe (the field step III), the magnetic domains grow mainly by elongation as shown in Fig. 1 (d). Contiguous domain structures of maze-type can be seen in the field step IV from 0 to -200 Oe as seen in Fig. 1 (e), where neighboring magnetic domains begin to connect with each other as the magnetic domains are densely crowed. Here, the magnetization reversal mostly proceeds by domain wall propagation rather than domain nucleation.

In Fig. 1, it is worth pointing out that magnetic domains are reversed with the sequence of Barkhausen avalanches at each field step. Under a given field, Barkhausen avalanches are fully accomplished according to the local field until the system is stable. The change of an external field stimulates Barkhausen avalanches in next step. To visualize Barkhausen avalanches occurred for each field step, we have subtracted the domain configuration image taken at the initial field of the step from one at the final field of the step. In Fig. 2, we demonstrate the two-dimensional distribution of Barkhausen avalanches existed in each field step together with domain configuration images taken at five different applied fields in the descending branch of the hysteresis loop, where the colors from blue to red indicate the field steps I, II, III, and IV, respectively. The discrete Barkhausen avalanches randomly distributed on the sample surface are clearly visible.

Interestingly, the size and shape of Barkhausen avalanches are noticeably changed according to the field step. In the field step I, jagged Barkhausen avalanches of small size in the distance are observed. As the field step turns toward IV, large elongated avalanches at close hand are mostly witnessed than small jagged Barkhausen avalanches. Considering the fact that the small jagged and large elongated avalanches are outcomes of Barkhausen avalanche process by domain growth and domain wall propagation, respectively, different size and shape of Barkhausen avalanches for each field step reflect the abstruse magnetization reversal process along the hysteresis loop in CoCrPt alloy film.

A critical issue in Barkhausen avalanches during magnetization reversal is their random behavior in repeated cycles, since the repeatability of hysteretic phenomena in magnetization reversal process is essential for achieving high performance of magnetic recording. To investigate the random behavior of Barkhausen avalanches, magnetic domain configurations were recorded at the same sample area in several hysteretic cycles. A topological line defect on the sample surface was used to confirm the exact same location in the sequential experiments. Figure 3 (a) displays domain configurations taken at applied magnetic fields of +600, +400, +200, 0 and -200 Oe in two consecutive hysteretic cycles. Barkhausen avalanches occurred during the four field steps in the two consecutive experiments are presented in Fig. 3 (b). Note that Barkhausen avalanche distribution shows the randomness of location in two successive measurements carried out under the same experimental conditions. Based on the fact that Barkhausen avalanches are started from domain nucleation sites, the random nature in location of Barkhausen avalanches in repeated cycles can be understood as a result of thermal effect on magnetization reversal process [25].

The most fundamental question is what kind of the statistical nature exists in the randomness of Barkhausen avalanches. To answer for this question, we have systematically investigated Barkhausen avalanches for each field step; the magnetic domain configurations were repeatedly measured in several tens of successive hysteretic cycles at the exactly same area of the sample. The size of individual avalanche was determined by counting of the pixels in reversed area corresponding to Barkhausen avalanche using particle-analysis software. The sizes of more than 700 Barkhausen

avalanches were obtained for each field step. Through a statistical analysis of the size of Barkhausen avalanche, we found that the average size of Barkhausen avalanches increases and the distribution of avalanche sizes broaden as the field step moves from I to IV. The distributions of Barkhausen avalanche size for the four field steps are plotted on a log-log scale in Fig. 4. The inserted figures are superimposed image of two domain configurations taken at the initial and final fields of each step. The distribution of Barkhausen avalanche size reveals non-trivial fluctuation of power-law scaling distribution with constant scaling exponent at every field steps, which implies that the critical scaling is existed at all field steps until near the coercive field (~±300 Oe) in CoCrPt alloy film, despite their different size and shape in each field step. A notable point in Fig. 4 is the cutoff of avalanche distribution observed at all field steps, which is still a substantial question under debate about its origin. Disorder [2,5], finite-size of field of view [7,8,20,21], or a demagnetizing field [3,6] effects have been suggested as the candidates for the origin of the cutoff. Moreover, in avalanche size distributions of Fig. 4, one can sees the subtle change of cutoff size in the field step IV compared with ones in the field steps I, II, and III. In this system, numerous defects due to compositional segregation present a broad distribution of energy barriers, which exhibit a different statistic for a given field. In a weak reversing field, most defects play a role as pinning sites, whereas few defects with high-energy barrier overcoming the field strength are participating to wall pinning in a strong reversing field. Hence, the delicate change of cutoff size observed in the field step IV might be attributed to the consequence that the external field near coercive field is strong enough to exceed the most energy barriers induced by defects, thus the circumstance with relatively small disorder is generated in the field step [2,5]. And, the cutoff of avalanche distribution in this system is believed to be originated from disorder effect.

The most remarkable feature in the scaling behavior of Barkhausen avalanches along the hysteresis loop is the fact that the scaling exponent, which is a key parameter for description of complex avalanche phenomena, is unexpectedly altered in field step IV. The distributions of Barkhausen avalanche size are fitted with the scaling exponent of 1.02 ± 0.02, 0.96 ± 0.04, 0.98 ± 0.03, and 1.47 ± 0.03, respectively. The scaling exponents of avalanche size distributions in the field steps I, II, and III are nearly same of

~1 within the measurement error, while the value is 1.47 ± 0.03 in the field step IV. This result implies that the critical scaling behavior of Barkhausen avalanches undergoes a change from their usual behavior at specific field region around the coercive field. We interpret the unusual change of the scaling exponent in the particular field step IV by coupling among neighboring magnetic domains due to a high-density magnetic domains under this field step, yielding additional contribution to Barkhausen avalanche process. Barkhausen avalanches indicated by the green circles in overlapped domain configuration of Fig. 4 (d) clearly show that the numbers of Barkhausen avalanches are generated by combinations of adjacent domains, which only exists in the field step IV. The domain coupling by interaction among neighboring domain walls in the field step IV is believed to impose restriction on ordinary Barkhausen avalanche process, which results in an unusual scaling behavior. On the other hand, Barkhausen avalanche processes under the field steps I, II, and III are free from extra intervention and thus their natural characters are shown up in these field steps. The metamorphosis of the statistical behavior of Barkhausen avalanches at a specific field region is symbolic of complex and unpredictable phenomena in magnetization reversal process of actual 2D ferromagnetic system, which has been overlooked in theoretical studies on Barkhausen avalanches in ideal systems.

In summary, we have investigated the random nature of Barkhausen avalanches for every field step along the hysteresis loop in CoCrPt alloy film having perpendicular magnetic anisotropy via direct observation of magnetic domains with a 15-nm spatial resolution. A power-law scaling behavior is found to govern the randomness of Barkhausen avalanches for every field step, despite their different patterns for each field step. Additional contribution by domain coupling to Barkhausen avalanche process is found to be a part of the cause in the unpredicted alteration of the critical scaling behavior observed in the particular field step near the coercivity.

Acknowledgements

This work was supported by the Director, Office of Science, Office of Basic Energy Sciences, of the U.S. Department of Energy under Contract No. DE-AC02-05CH11231, Korea Science and Engineering Foundation through the Basic Research Program and the National Research Laboratory Projec, Ministry of Education, Science and Technology through the Global Partnership Program. This work was also supported by the research grant of the Chungbuk National University in 2007 and by the Korea Research Foundation Grant funded by the Korean Government (MOEHRD, Basic Research Promotion Fund) (KRF-2007-331-C0097).

References and Notes

[1] H. Barkhausen, Z. Phys. **20**, 401 (1919).
[2] J. P. Sethna *et al*., Phys. Rev. Lett. **70**, 3347 (1993).
[3] G. Durin and S. Zapperi, Phys. Rev. Lett. **84**, 4075 (2000).
[4] J. S. Urbach, R. C. Madison, and J. T. Markert, Phys. Rev. Lett. **75**, 276 (1995).
[5] J. P. Sethna, K. A. , Dahmen, and C. R. Myers, Nature **410**, 242 (2001).
[6] S. Zapperi, P. Cizeau, G. Durin, and H. E. Stanley, Phys. Rev.B **58**, 6353 (1998).
[7] K.-S. Ryu, H. Akinaga, and S.-C. Shin, Nature Phys **3**, 547 (2007).
[8] D.-H. Kim, S.-B. Choe, and S.-C. Shin, Phys. Rev. Lett. **90**, 87203-1 (2003).
[9] E. Puppin, Phys. Rev. Lett. **84**, 5415 (2000).
[10] A. Sharoni, J. G. Ramirez, and I. K. Schuller, Phys. Rev. Lett. **101**, 026404 (2008).
[11] S. Field, J. Witt, F. Nori, and X. Ling, Phys. Rev. Lett. **74**, 1206 (1995).
[12] D. S. Fisher, Phys. Rev. Lett. **50**, 1486 (1983).
[13] G. Durin and S. Zapperi, in *The Science of Hysteresis*, edited by G. Bertotti and I. Mayergoyz (Academic, New York, 2005), pp. 181-267.
[14] A. Berger, A. Inomata, J. S. Jiang, J. E. , Pearson, and S. D. Bader, Phys. Rev. Lett. **85**, 4176 (2000).
[15] O. Narayan, Phys. Rev. Lett. **77**, 3855 (1996).
[16] F. Pazmandi, G. Zarand, and G. T. Zimanyi, Phys. Rev. Lett. **83**, 1034 (1999).
[17] M. Mansuripur, *The Physical Principles of Magneto-optical Recording* (Cambridge University Press, New York, 1995), pp. 543-676.
[18] A. Hulbert and R. Schaefer, *Magnetic Domains* (Springer, Berlin, 1998).
[19] R. Ramesh and K. Srikrishna, J. Appl. Phys. **64**, 6406 (1988).
[20] P. Bak, C. Tang, and K. Wiesenfeld, Phys. Rev. Lett. **59**, 381 (1987).
[21] P. J. Cote and L. V. Meisel, Phys. Rev. Lett. **67**, 1334 (1991).
[22] O. Perkovi´c, K. Dahmen, and J. P. Sethna, Phys. Rev. Lett. **75**, 4528(1995).
[23] A. Schwarz, M. Liebmann, U. Kaiser, and R. Wiesendanger, Phys. Rev. Lett. **92**, 077206-1 (2004).
[24] M.-Y. Im, P. Fischer, T. Eimüller, G. Denbeaux, and S. -C. Shin, Appl. Phys. Lett. **83**(22), 4589 (2003).
[25] M.-Y. Im, P. Fischer, D.-H. Kim, K.-D. Lee, S.H. Lee, and S.-C. Shin, Adv. Mater. **20**, 1750 (2008).
[26] Y. Xu, J. P. Wang, and Y. Su, J. Appl. Phys. **87**, 6971 (2000).
[27] P. Fischer *et al.*, Materials Today **9**, 26 (2006).
[28] W. Chao, B. H. Harteneck, J. A. Liddle, E. H. Anderson, and D. T. Attwood, Nature **435**, 1210-1213 (2005).
[29] P. Fischer, D.-H. Kim, B. L. Mesler, W. Chao, A.E. Sakdinawat, and E. H. Anderson, Surface Science **601**, 4680 (2007).
[30] M.-Y. Im, D. -H. Kim, and S. -C. Shin, Phys. Rev. B **72**, 132416 (2005).

Figure Captions

FIG. 1. (a-e) Typical magnetic domain configurations of $(Co_{0.83}Cr_{0.17})_{87}Pt_{13}$ alloy film recorded at the Co L_3 absorption edge (777 eV) with applied magnetic fields of +600, +400, +200, 0, and -200 Oe. (f) M vs H hysteresis loop obtained via VSM measurement.

FIG. 2. (a-e) Magnetic domain configurations of $(Co_{0.83}Cr_{0.17})_{87}Pt_{13}$ alloy film taken at applied magnetic fields of +600, +400, +200, 0, and -200 Oe in the descending branch of the major hysteresis loop. (f) Two-dimensional distribution of Barkhausen avalanches observed in the field steps I, II, III, and IV.

FIG. 3. (a) Magnetic domain configuration sequences of $(Co_{0.83}Cr_{0.17})_{87}Pt_{13}$ alloy film taken at applied magnetic fields of +600, +400, +200, 0, and -200 Oe in the successive two hysteretic cycles. (b) Two-dimensional distributions of Barkhausen avalanches taken from each field step for the repetitive measurements.

FIG. 4. Distributions of the Barkhausen avalanche size taken in the field steps (a) I, (b) II, (c) III, and (d) IV along the hysteresis loop in $(Co_{0.83}Cr_{0.17})_{87}Pt_{13}$ alloy films, where each distribution was determined from the statistical analysis of more than 700 Barkhausen avalanche size. Each curve was determined from the least-mean-square fitting. The inserted images are superimposed domain configurations taken at the initial and final fields of each step.

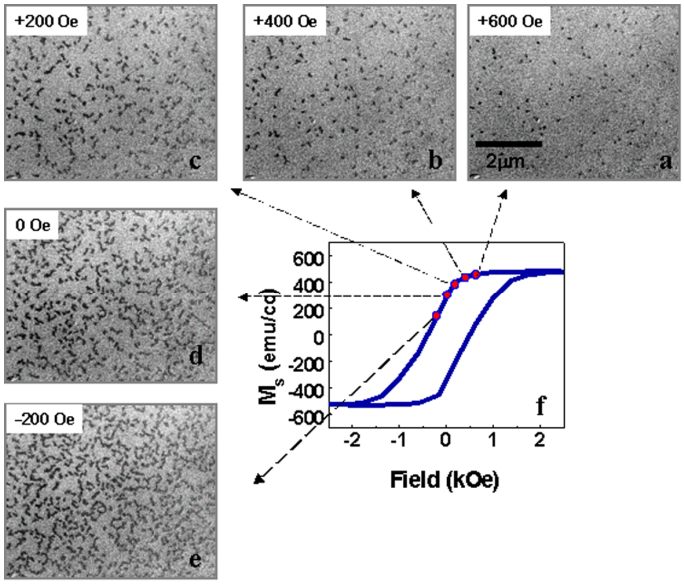
+200 Oe
+400 Oe
+600 Oe
c
b
2μm
a
0 Oe
d
-200 Oe
e
600
400
200
0
-200
-400
-600
M_s (emu/cc)
f
-2
-1
0
1
2
Field (kOe)

FIG. 1

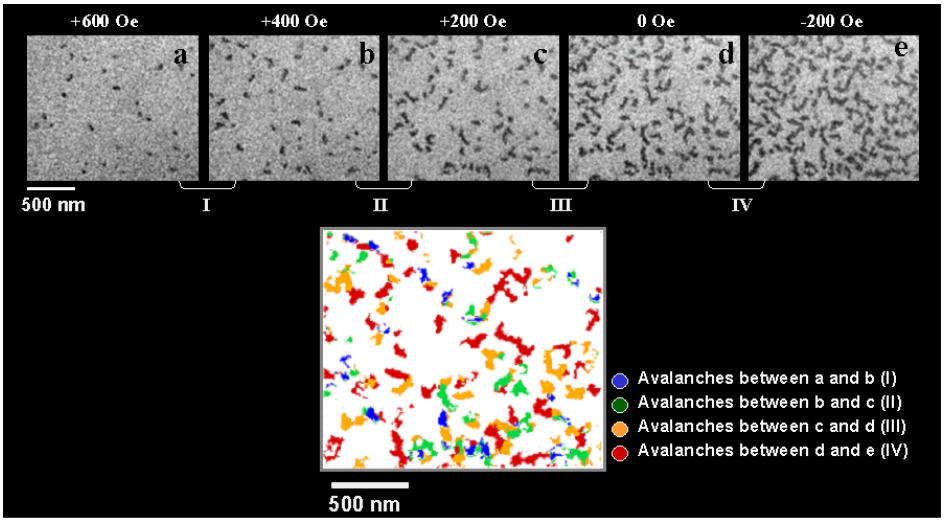
+600 Oe
+400 Oe
+200 Oe
0 Oe
-200 Oe
a
b
c
d
e
500 nm
I
II
III
IV
Avalanches between a and b (I)
Avalanches between b and c (II)
Avalanches between c and d (III)
Avalanches between d and e (IV)
500 nm

FIG. 2

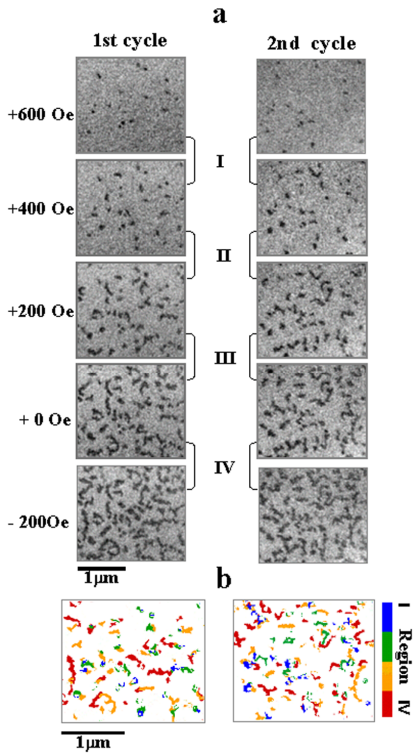
a
1st cycle
2nd cycle
+600 Oe
+400 Oe
+200 Oe
+ 0 Oe
- 200Oe
I
II
III
IV
1μm
b
1μm
Region I
Region IV

FIG. 3

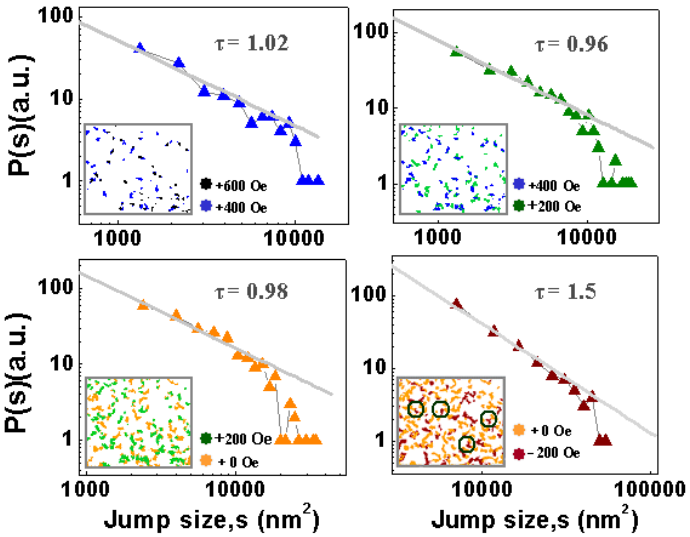
τ= 1.02
+600 Oe
+400 Oe
τ= 0.96
+400 Oe
+200 Oe
τ= 0.98
+200 Oe
+ 0 Oe
τ= 1.5
+ 0 Oe
- 200 Oe
P(s)(a.u.)
P(s)(a.u.)
100
10
1
1000
10000
100000
Jump size,s (nm²)
Jump size,s (nm²)

FIG. 4